



LAWRENCE
LIVERMORE
NATIONAL
LABORATORY

MINIMIZING DECOMPOSITION OF VAPORIZED HYDROGEN PEROXIDE IN CLEAN GALVANIZED STEEL DUCTING: IMPLICATIONS FOR BIOLOGICAL DECONTAMINATION

M. F. Verce, B. Jayaraman, T. D. Ford, S. E.
Fisher, A. J. Gadgil, T. M. Carlsen

September 18, 2007

MINIMIZING DECOMPOSITION OF VAPORIZED
HYDROGEN PEROXIDE IN CLEAN GALVANIZED STEEL
DUCTING: IMPLICATIONS FOR BIOLOGICAL
DECONTAMINATION

This document was prepared as an account of work sponsored by an agency of the United States Government. Neither the United States Government nor the University of California nor any of their employees, makes any warranty, express or implied, or assumes any legal liability or responsibility for the accuracy, completeness, or usefulness of any information, apparatus, product, or process disclosed, or represents that its use would not infringe privately owned rights. Reference herein to any specific commercial product, process, or service by trade name, trademark, manufacturer, or otherwise, does not necessarily constitute or imply its endorsement, recommendation, or favoring by the United States Government or the University of California. The views and opinions of authors expressed herein do not necessarily state or reflect those of the United States Government or the University of California, and shall not be used for advertising or product endorsement purposes.

1 **MINIMIZING DECOMPOSITION OF VAPORIZED HYDROGEN PEROXIDE**
2 **IN CLEAN GALVANIZED STEEL DUCTING:**
3 **IMPLICATIONS FOR BIOLOGICAL DECONTAMINATION**

4
5 MATTHEW F. VERCE,^{*,†,§} BUVANESWARI JAYARAMAN,[‡] TIMOTHY D.
6 FORD,^{†,§} SCOTT E. FISHER,^{†,§} ASHOK J. GADGIL,[‡] AND TINA M. CARLSEN[#]
7 Environmental Restoration Division, National Security Engineering Division, and
8 Biosciences and Biotechnology Division, Lawrence Livermore National Laboratory,
9 Livermore CA 94551 and Environmental Energy Technologies Division, Lawrence
10 Berkeley National Laboratory, Berkeley, CA 94720

11
12
13 * Corresponding author. Mailing address: L-530, Lawrence Livermore National
14 Laboratory, Livermore CA 94551. Phone: (925) 423 – 2129. Fax: (925) 424 – 3155.
15 Email: vercel@llnl.gov

16
17 [†] Environmental Restoration Division, Lawrence Livermore

18 [‡] Environmental Energy Technologies Division, Lawrence Berkeley

19 [§] National Security Engineering Division, Lawrence Livermore

20 [#] Biosciences and Biotechnology Division, Lawrence Berkeley

21

22

23

1 **Abstract**

2 This work examined the behavior of vaporous hydrogen peroxide (VHP) in clean,
3 room-scale galvanized steel (GS) and polyvinylchloride-coated steel air ducts, to
4 understand how it might be used to decontaminate larger ventilation systems. VHP
5 injected into the GS duct decreased in concentration along the length of the duct, whereas
6 VHP concentrations in the polyvinylchloride coated duct remained essentially constant,
7 suggesting that VHP decomposed at the GS surface. However, decomposition was
8 reduced at lower temperatures (~22°C) and higher flow rates (~80 actual cubic meter per
9 hour). A computational fluid dynamics model incorporating reactive transport was used
10 to estimate surface VHP concentrations where contamination is likely to reside, and also
11 showed how bends encourage VHP decomposition. Use of *G. stearothermophilus*
12 indicators, in conjunction with model estimates, indicated that a concentration-contact
13 time of ~100 mg/L H₂O₂(g)•min was required to achieve a 6 log reduction of indicator
14 spores in clean GS duct, at 30°C. When VHP is selected for building decontamination,
15 this work suggests the most efficacious strategy may be to decontaminate GS ducting
16 separately from the rest of the building, as opposed to a single decontamination event in
17 which the ventilation system is used to distribute VHP throughout the entire building.

18

19 **Introduction**

20 The deaths and widespread contamination resulting from the incident in the
21 United States in 2001, in which spores of the highly virulent *B. anthracis* Ames strain
22 were sent via mail to various destinations (1, 2), highlighted the need for an improved
23 understanding of biological decontamination of buildings and their interiors. The

1 ventilation system inside a contaminated building is likely to become contaminated as
2 well, either by direct introduction of a biological warfare agent, or indirectly by
3 reaerosolization of spores (3) in rooms to which the system is connected. Once inside a
4 ventilation system, spore transport can be influenced by a number factors, including size
5 (4, 5), duct material (5, 6), and connectors and bends in the duct (7). Depending on its
6 accessibility and value of associated hardware, demolition and disposal of a contaminated
7 ventilation system may be prohibitively expensive. Therefore, a need exists to
8 decontaminate high value ventilation systems *in situ*, if they become contaminated with a
9 biological agent.

10 Gaseous fumigants are a natural choice for decontaminating ducts, because they
11 can be introduced at an accessible location and then allowed to permeate into the remote
12 reaches of a ventilation system. Several fumigants can be considered for this purpose,
13 including paraformaldehyde, methyl bromide, vaporized hydrogen peroxide (VHP), and
14 chlorine dioxide gas (1). The present work investigated the use of VHP (8), because it is
15 widely used to decontaminate clean rooms (9, 10), decomposes into the innocuous end
16 products water and molecular oxygen, and recently has been modified to decontaminate
17 chemical warfare agents (11). Furthermore, it can be scaled up to decontaminate large
18 buildings (12, 13), and was used to decontaminate some of the buildings contaminated
19 during the incident in the United States in 2001 (1).

20 The overall objective of this work was to determine how the behavior of VHP
21 inside galvanized steel ducting might affect the decontamination of a biological warfare
22 agent. The specific tasks undertaken were to: assess the effect of galvanized steel (GS), a
23 common duct material, on VHP concentrations within a room-scale air duct; measure

1 VHP concentrations as a function of operating parameters that practically can be adjusted
2 during a decontamination event, including temperature, flow rate, and VHP injection rate;
3 measure concentration-contact time (C•t) values required to kill biological indicators
4 (BIs) of *Geobacillus stearothermophilus* spores, a surrogate for *B. anthracis* spores,
5 within the GS duct; develop and calibrate a computational fluid dynamics (CFD) model
6 to predict VHP concentrations at any location within the duct; use the CFD model to
7 understand how bends in a GS duct effect VHP concentration; and to illustrate how BI
8 kill and CFD results can be used to estimate decontamination times for ducts.

9

10 **Materials and Methods**

11 **Experimental apparatus.** Decontamination experiments were conducted in two
12 adjacent rooms of a retrofitted construction trailer, housing a model duct run and required
13 instrumentation, respectively. Separate duct runs were constructed of round, 6 in (15.2
14 cm) diameter GS “snap duct” (obtained from a local building supply store) or
15 polyvinylchloride (PVC)-coated steel duct (McMaster-Carr). A layout was chosen (Fig.
16 1) to make the duct as long as practically possible, within the space of the test room.
17 VHP produced by a STERIS VHP 1000[®] generator was introduced into one end of the
18 duct, and was measured at six locations along the duct with near-infrared spectroscopy
19 (Guided Wave Model 412 Process Analyzer; reference 14) by absorption cells (25 cm
20 path length) placed normally to the duct’s axis (inset, Fig. 1) at each location. The
21 STERIS VHP 1000[®] generator was the source of flow for the majority of experiments
22 (~21 actual cubic meter per hour (acmh)). Higher flow rates were achieved by
23 connecting a dust collector (Dayton model 6H004A) to the end of the duct. Temperature

1 at each absorption cell was measured by a thermistor (Omega, model THX400AP)
2 protruding into the duct, and flow rates were measured by “machined convergent” type
3 venturis placed at the end of the duct. Experiments were nearly isothermal, with
4 temperatures decreasing by a maximum of 3°C along the length of the duct.

5 **Safety.** Workers were protected from exposure to VHP by making the room
6 containing the duct as air tight as practically possible, and running experiments remotely
7 from the adjacent room, which was maintained at a slightly higher relative air pressure.
8 VHP concentrations in the adjacent room also were monitored by a Drager PAC III
9 electrochemical detector alarmed at 1 ppmv.

10 **VHP profile experiments.** VHP profiles were measured separately in GS and
11 PVC-lined steel ducts at various initial VHP concentrations entering the duct, flow rates,
12 and temperatures (Table 1). The liquid hydrogen peroxide sterilant vaporized by the
13 STERIS VHP 1000[®] generator was either a 35% solution (Vaprox[®], STERIS), or a 14%
14 solution (obtained by dilution) to achieve lower VHP concentrations. All experiments
15 were run for a minimum of four hours (six hours was common), to ensure steady state
16 values were reached throughout the entire duct. For each set of conditions tested, three
17 experiments were performed on separate days, and VHP concentrations were reported as
18 a weighted average calculated by

19
$$\sum_i \frac{\bar{C}_i}{s_i^2} / \sum_i \frac{1}{s_i^2} \quad (1)$$

20 where \bar{C}_i and s_i are the steady state average and standard deviation, respectively of VHP
21 concentrations from a given experiment (15).

22 **C•t values.** C•t values were estimated with BIs containing approximately 2.5E6
23 *G. stearothermophilus* spores (Apex Labs, lot H0635) placed inside the GS duct, in the

1 immediate vicinity of the first and fifth absorption cells (Fig. 1). *G. stearothermophilus*
2 spores were chosen because they are more resistant to VHP than spores of many other
3 bacteria (16 - 19), including *B. anthracis* Ames strain (20). For each experiment, ten BIs
4 were taped to a plastic strip that conformed to the inside of the duct, and three replicate
5 experiments were performed for each exposure time. These tests were performed
6 separately from those described above, but under the same nominal conditions of 20
7 acmh and 30°C. After a given exposure time, BIs were collected from the duct, placed
8 aseptically into prepared tryptic soy broth tubes (PML Microbiologicals), incubated for 7
9 days at 55°C, and then inspected visually for turbidity as a sign of growth.

10 **Modeling VHP Fate and Transport.** CFD simulation of the loss of VHP within
11 the GS duct was performed using the commercial software STAR-CD (CD-Adapco)
12 using the second-order Monotone Advection Reconstruction Scheme (21) and the
13 SIMPLE algorithm (22). General boundary conditions included a laminar, plug flow
14 velocity at the duct's entrance, isothermal walls, and setting the VHP mass entering the
15 duct equal to the product of the experimentally measured flow rate and concentration at
16 the first absorption cell (Fig. 1). A computational grid consisting of 817,000 cells was
17 constructed for the duct configuration shown in Fig. 1. Local mesh refinement was
18 carried out close to the walls, resulting in a maximum non-dimensional normal distance
19 (y^*) from the wall of 0.6. The finite volume formulation of the Reynolds Averaged
20 Navier Stokes equations

$$\frac{\partial U_i}{\partial x_j} = 0 \quad (2)$$

$$U_j \frac{\partial U_i}{\partial x_j} = -\frac{1}{\rho} \frac{\partial p}{\partial x_i} + \frac{\partial}{\partial x_j} \left(\mathbf{v}_{total} \frac{\partial U_i}{\partial x_j} \right) + \frac{\partial \tau_{ij}}{\partial x_j} \quad (3)$$

were solved to predict the steady-state airflow field in the duct. Turbulence was included via stress tensor elements (τ_{ij} , Supporting Information) determined by integrating the low-Reynolds-number turbulence model

$$U_j \frac{\partial k}{\partial x_j} = \frac{\partial}{\partial x_j} \left(\mathbf{v}_{total} \frac{\partial k}{\partial x_j} \right) + \mathbf{v}_{turb} P - \varepsilon \quad (4)$$

$$U_j \frac{\partial \varepsilon}{\partial x_j} = \frac{\partial}{\partial x_j} \left(\mathbf{v}_{molec} + \frac{\mathbf{v}_{turb}}{1.22} \frac{\partial \varepsilon}{\partial x_j} \right) + \frac{\varepsilon}{k} 1.44 \mathbf{v}_{turb} (P + P') - 1.92 \left(1 - 0.3e^{-R_i^2} \right) \frac{\varepsilon^2}{k} \quad (5)$$

all the way to the wall of the duct (as opposed to assuming a wall function). Lastly, the VHP concentrations were predicted for a given airflow field by solving the transport equation

$$U_j \frac{\partial C}{\partial x_j} + \frac{\partial}{\partial x_j} \left(C \mathbf{v}_{m,j} + \overline{u'_j C'} \right) = S \quad (6)$$

where S is a sink term due to VHP decomposition, which was set equal to

$$S = -\frac{K_1 C}{K_2 + C} \quad (7)$$

1
2 in the first layer of cells adjacent to the wall, and zero everywhere else. The mixed order
3 form of Eq. 7 was suggested by data collected at different initial VHP concentrations
4 (Results), which indicated a uniform loss rate at the highest concentrations tested, and a
5 first order loss at lower concentrations. Several simulations of each VHP data set were
6 performed, until one set of values for K_1 and K_2 was obtained that resulted in an
7 acceptable root mean square error. All terms in the above equations are summarized in
8 Nomenclature.

9

10 **Results**

11 **Qualitative effect of VHP on GS.** Oxidative damage to the GS duct was
12 minimal, even after performing more than 100 experiments over a one year period. A
13 visual examination of the GS duct when it was dismantled revealed a patina on surfaces
14 in the immediate vicinity of where VHP was introduced, but most of the duct had a
15 mildly dulled or hazed appearance, compared to GS not exposed to VHP.

16 **Duct material and process parameter effects.** Reproducible data from the GS
17 duct were obtained after initial passivation of the GS duct during several preliminary
18 experiments (data not shown). Results of experiments performed at different VHP mass
19 loading rates (or equivalently, different initial VHP concentrations entering the duct) with
20 GS and PVC-lined steel ducts are shown in Fig. 2. As can be seen, VHP concentrations
21 decreased markedly along the length of the GS duct (Fig. 2a), but were essentially
22 constant in the PVC-lined duct tested under the same nominal conditions (Fig. 2b). VHP
23 concentrations in GS duct were also dependent on flow rate (Fig. 3) and temperature (Fig.

1 4). To determine the effect of each parameter, the percent VHP loss was calculated as the
2 ratio of VHP mass exiting the duct to the total VHP mass vaporized by the generator
3 during each set of experiments (Table 1). As can be seen, the highest flow rate (~78
4 acmh) and the lowest temperature (~22°C) tested led to the smallest percent losses within
5 the GS duct. Increasing the initial VHP concentration with other parameters held
6 constant also minimized VHP loss, but not to the same extent (Table 1). VHP losses
7 were the largest at the lowest initial concentration and highest temperature tested (Table
8 1).

9 **VHP decomposition rates.** The attenuation of VHP in the GS duct, but minimal
10 attenuation in the PVC-lined duct under the same conditions, suggested that the GS was
11 catalyzing the decomposition of VHP at the surfaces of the duct. To test this hypothesis,
12 the three dimensional CFD model incorporating reaction at the GS surface was used to
13 simulate the VHP data (dotted lines in Figs. 2-4). Due to the temperature sensitivity of
14 VHP decomposition, separate CFD simulations were performed to obtain values of K_1
15 and K_2 at each temperature tested (Table 2). The coefficients at ~30°C were determined
16 by simulating data at lower (Fig. 2a) and higher (Fig. 3) flow rates simultaneously to
17 obtain one representative set of coefficients for this temperature, as opposed to fitting
18 them separately. The agreement between measured and CFD predicted VHP
19 concentrations was reasonable for all temperatures except ~ 30°C, for which agreement
20 was better at lower flow rates (e.g. Fig. 2a) than at higher ones (Fig. 3).

21 Surface area normalized decomposition rates were estimated by dividing the VHP
22 loss rate, given by Eq. 7, by the surface area of the grid cell at a particular location. The
23 largest decomposition rates observed in this study (Table 2) were estimated at the

1 beginning of the duct where VHP surface concentrations, and therefore decomposition,
2 were the highest. These rates may not be maximal, however, because some experiments
3 were initiated at VHP concentrations near or below the value of K_2 (Table 2), implying
4 decomposition rates (e.g. Eq. 7) may not have reached maximum values. Fit of an
5 Arrhenius-like expression ($K_A=A\exp(E_a/RT_K)$) to surface area normalized decomposition
6 rates (K_a ; Table 2) yielded a pre-exponential factor (A) of 6.2E13 nanomole/min/cm² and
7 an activation energy (E_a) of 68.8 kJ/mol (with a R^2 of 0.99; data not shown).

8 **Effect of bends in GS duct.** Once values for K_1 and K_2 were obtained, the CFD
9 model was used to understand the effect of bends on VHP concentration within the GS
10 duct. Using the first bend as an example, CFD predicted the VHP profile exiting the
11 bend was altered, and of a lower average value, than that entering the bend (Fig. 5a).
12 VHP loss occurs at every bend, so that after ~ 1.5 m the actual duct tested (Fig. 1) was
13 predicted to have lower concentrations than a straight duct (Fig. 5b) of equal length. In
14 general, fluid flow around a bend creates regions of lower and higher velocity on the
15 bend's inner and outer edges, respectively (23), the net result of which is more destruction
16 of VHP in the bend, compared to regions of straight duct with fully developed flow (Fig.
17 5b).

18 **Surface VHP concentrations.** One straightforward outcome of a surface
19 catalyzed decomposition process is a decrease in VHP concentrations contacting the
20 surface. Again using the first bend in the GS duct as an example, the VHP concentrations
21 contacting the walls of the duct (e.g. at axial distances 0 cm and 15.24 cm, Fig 5a) were
22 appreciably lower than the bulk concentration at this location. This is illustrated further
23 in Fig. 6, which shows the surface concentrations were predicted to be lower than bulk

1 concentrations throughout the entire duct. These results highlight the fact that measured
2 VHP concentrations are much closer to the bulk concentration in the middle of the duct
3 than those contacting the surface, because they are average values measured across the
4 path length of a particular absorption cell.

5 **C•t values and estimated decontamination times.** C•t values at the first and
6 fifth absorption cells (Fig. 1) were estimated as the product of the exposure time required
7 to kill BIs and the surface VHP concentration (obtained by CFD) at each location. The
8 results are shown in Fig. 7, which indicates a minimum C•t value of 83 mg/L•min (0.925
9 mg/L•90 min) was required to kill all BIs placed at the first absorption cell (Fig. 7a),
10 whereas a value greater than 100 mg/L•min (0.185 mg/L•540 min) may have been
11 required at the fifth absorption cell (Fig. 7b). The positive result at the fifth absorption
12 cell at 100 mg/L•min (Fig. 7b) was due to the growth of one BI out of thirty. These C•t
13 values correspond to a 6 log reduction of indicator organisms under the conditions tested,
14 because the BIs had a burden >2E6 spores.

15 One way to estimate the time required to decontaminate an air duct is to
16 determine the time at which the entire inner surface of the duct exceeds a given C•t value.
17 For this approach, CFD can provide the VHP concentrations contacting the surface where
18 spores would likely reside, and the C•t value used must be representative of the
19 conditions inside the duct. This is illustrated for the GS duct in Fig. 8, which compares
20 the decontamination time for experiments performed at the highest flow rate (open
21 triangles, Fig. 3) with that of experiments performed at the highest initial concentration
22 (open circles, Fig. 2a). As can be seen, conditions associated with the highest flow rate
23 tested (curve a, Fig. 8) decontaminated the GS duct approximately three times faster than

1 those associated with the highest initial concentration (curve b, Fig. 8). This illustration
2 assumed a constant $C \cdot t$ value (e.g. “Chick-Watson” or “toxic load” exponent equal to
3 one; reference 24) of 100 mg/L•min determined from BI experiments (above). The two
4 curves in Fig. 9 cross because the VHP concentrations at the highest flow rate tested
5 initially were lower in the first ~ 12 m of the duct (Fig. 2a), but then were higher in the
6 remaining length of the duct, compared to experiments at the highest initial concentration
7 tested (Fig. 3).

8

9 Discussion

10 The observations of decreasing VHP concentrations along the length of the GS
11 duct under a variety of conditions, but essentially constant VHP concentrations along the
12 length of the PVC-lined duct, strongly indicate that VHP undergoes a surface catalyzed,
13 heterogeneous decomposition as it passes through GS ducting. Clearly, the loss observed
14 in the GS duct was not due to homogeneous decomposition of VHP, which occurs only at
15 temperatures greater than 400°C (25). Heterogeneous decomposition of VHP has been
16 reported qualitatively at near-ambient temperatures (26, 27). VHP decomposition rates
17 also have been measured at temperatures between 110°C-250°C, and ranged between 1
18 $\mu\text{mole H}_2\text{O}_2/\text{min}/\text{cm}^2$ for glass to greater than 100 $\mu\text{mole H}_2\text{O}_2/\text{min}/\text{cm}^2$ for
19 electropolished stainless steel (28). Although the decomposition rates for GS duct
20 reported in the present study at ambient temperatures (40-167 nmol $\text{H}_2\text{O}_2/\text{min}/\text{cm}^2$; Table
21 2) are at least two orders of magnitude smaller than those reported at higher temperatures,
22 the very large surface area of a typical duct system is likely to cause a substantial loss of
23 VHP that will impact decontamination. VHP is not unique in its reaction and depletion at

1 surfaces. Other fumigants, including chlorine dioxide (29) and ozone (30) also are
2 consumed by surfaces found in the indoor environment, although the effect of GS on
3 these other fumigants apparently has not yet been reported.

4 Though VHP decomposition is catalyzed by GS surfaces, the results presented
5 here show it can be minimized by the choice of operating conditions during
6 decontamination. Temperature, flow rate, and initial concentration each effected the
7 fraction of VHP mass decomposed, with temperature and flow rate having the most
8 beneficial effect over the ranges tested (Table 1). Lower temperatures slowed the
9 kinetics of VHP decomposition, as suggested by the reasonable fit of K_A (Table 2) to an
10 Arrhenius- like expression. In general, higher flow rates are expected to result in two
11 competing effects: increased turbulent transport of VHP to the duct's surface, which
12 feeds the decomposition reaction; and decreased residence time of VHP within the duct
13 to react with the GS surface. For the duct system in the present work, shorter residence
14 times apparently were more important in determining the effect of flow rate. For
15 building scale applications, lower temperatures could be created with a cooling system or
16 simply by operating in the coolest parts of the day, provided condensation is managed
17 properly. Higher flow rates are easily produced with large blowers, but would require a
18 larger VHP generator (12) to maintain sporicidal concentrations. It should not be
19 assumed, however, that conditions minimizing VHP decomposition will necessarily
20 decrease the time required for decontamination. For example, lower temperatures also
21 may slow the kinetics of VHP killing spores, as observed in liquid H_2O_2 solutions (31,
22 32). Clearly, minimizing decomposition makes more VHP available for

1 decontamination, but actual decontamination times are estimated most accurately with
2 C•t values measured at operating conditions.

3 The VHP decomposition kinetics observed in these experiments were limited
4 mainly by the rate of reaction at the surface of the GS duct, and to a lesser extent by the
5 transport of VHP to the duct's surface. This is indicated by the dramatic effect of
6 temperature, because temperature directly affects decomposition rate, while minimally
7 affecting turbulent transport. Furthermore, higher flow rates, which should enhance
8 transport of VHP to the surface, actually decreased the fraction of VHP decomposed
9 (Table 1). This suggests the fitted coefficients and rates listed in Table 2 largely are
10 independent of transport effects unique to this experiment, and capture the kinetics of
11 VHP decomposition at the GS surface tested. Of course, to develop a predictive
12 engineering capability for duct decontamination, kinetic coefficients for a variety of
13 indoor surfaces, including surfaces soiled with typical indoor dust and grime, should be
14 obtained.

15 The present work attempted to capture the effect of VHP decomposition on
16 biological decontamination by placing commercial BIs within the duct, but clearly this is
17 different from killing aerosolized spores in an aged duct after a spectacular event. In a
18 recent survey of indoor materials (20), the log reduction of *G. stearothersophilus* spores
19 was approximately five times lower than *B. anthracis* Ames strain spores when both were
20 inoculated onto coupons of GS, meaning *G. stearothersophilus* is a good indicator for
21 decontamination of GS surfaces. However, *G. stearothersophilus* on GS coupons also
22 were much more resistant than commercial *G. stearothersophilus* BIs made from
23 stainless steel coupons (20) similar to those used in the present work. Furthermore, the

1 GS duct used in the present study was new and passivated, whereas functioning
2 ventilation systems contain dust, grime, and other materials that will most likely exert an
3 additional oxidative demand for VHP. Therefore, the C•t values presented here very
4 likely underestimate actual values required to decontaminate aged GS duct in a building.

5 CFD analysis yielded information on two additional aspects that effect VHP
6 decontamination of GS ducting. First, CFD simulations provided quantitative estimates
7 of VHP concentrations at the surface of the duct, as opposed to average, near-bulk
8 concentrations provided by the experiments. This is an important distinction because
9 spores are likely to settle on the interior surfaces of the duct (5, 6). Most commercially
10 available detectors for the major fumigants measure only bulk concentrations, and CFD
11 provides a general way to estimate the corresponding surface concentrations. Second,
12 CFD showed quantitatively how bends enhance VHP decomposition. Given the catalytic
13 nature of GS towards VHP, this finding is consistent with the general observation that
14 bends in pipes enhance heat and mass transport (33). Furthermore, CFD simulations can
15 be used to predict the time required for decontaminating a duct, including the effects of
16 bends. It is recognized that CFD cannot be applied to every ventilation system that may
17 require decontamination. Rather, this work suggests that CFD analysis of a limited
18 number of additional experiments, involving different duct materials and geometries,
19 could provide average reaction rates that would reasonably predict decontamination in a
20 wide variety of ventilation systems.

21 This work has bearing on the larger issue of whether or not ventilation systems
22 should be used to distribute gaseous decontaminants throughout an entire building, as
23 was done with chlorine dioxide during decontamination of the US Postal Service's

1 Trenton facility in 2003 (34). This approach may not be suitable for VHP, if
2 decomposition within the duct significantly reduces the concentration delivered to
3 attached rooms and spaces. However, the ventilation system could be isolated from the
4 building and decontaminated separately to insure adequate concentrations are reached, as
5 was done during the successful decontamination of the General Services Administration's
6 Building 410 with VHP in 2003 (35). Decontaminating a ventilation system with VHP
7 separately from the rest of the building is an additional step that stakeholders may want to
8 take, if the possible corrosive effects of chlorine dioxide (36) on the ventilation system
9 are a concern.

10

11 **Acknowledgements**

12 This work was performed under the auspices of: the U.S. Department of Energy
13 by University of California at Lawrence Livermore National Laboratory (experiments;
14 Contract W-7405-Eng-48) and Lawrence Berkeley National Laboratory (modeling;
15 Contract DE-AC02-05CH11231), both of which were funded by the Department of
16 Homeland Security; and a Cooperative Research and Development Agreement with
17 Strategic Technology Enterprises Inc., a subsidiary of STERIS Corp. The efforts of
18 Catherine Elizondo and Lew Schwartz to establish the Cooperative Research and
19 Development Agreement are gratefully acknowledged. Jim Thomas and Iain McVey
20 provided helpful insight into the experimental setup and discussion of results. Tracy
21 Thatcher and Jennifer McWilliams performed a blower door analysis of the test facility.
22 Diana Warden helped perform initial duct experiments, and Lianna Balser assisted with
23 BI experiments. Phillip Price and Henrik Wallman provided valuable guidance on CFD

1 modeling and related statistical topics. George Metzger provided valuable assistance
2 with venturi flow measurements. Ron Fertig developed the LabVIEW data acquisition
3 system. Michael Feldman assisted with CFD modeling. Review comments of William
4 Smith, Michael Sohn, and Phillip Price are greatly appreciated.

5

6 **Supporting Information Available**

7 Additional details of the experimental apparatus, CFD modeling, and the effect of bends
8 on VHP decomposition. This material is available free of charge via the internet at
9 <http://pubs.acs.org>.

10

11 **Nomenclature**

- 12 A Arrhenius pre-exponential factor (nanomole/min/cm²)
13 C concentration of VHP (mg/L)
14 \bar{C}_l steady state average VHP concentration from a given experiment
15 C' fluctuating components of concentration
16 $C \cdot t$ Product of VHP concentration and exposure time (mg/L•min)
17 K_a Surface area normalized VHP decomposition rate (nmol/min/cm²)
18 K_1 zeroth order VHP decomposition constant (mg/L/sec)
19 K_2 VHP concentration at half maximum rate (mg/L)
20 k turbulent kinetic energy (m²/sec²)
21 P production of turbulent kinetic energy k , by mean velocity gradients
22 P' near-wall turbulence energy dissipation
23 p pressure (Pa)

1	R	Universal gas constant (8.3144 J/°K/mol)
2	R_t	turbulent Reynolds number
3	s_i	standard deviation of VHP concentration from a given experiment
4	T_K	Temperature (°K)
5	t	time (sec)
6	u'_i	fluctuating velocity component (m/sec)
7	U_i	mean velocity component (m/sec)
8	$V_{m,j}$	diffusion velocity component (m/sec)
9	x_i	Cartesian coordinate ($i=1, 2, 3$) (m)
10	y^+	non-dimensional normal distance from the wall
11	ε	turbulent dissipation rate (m ² /sec ³)
12	ν_{total}	total kinematic viscosity (m ² /sec)
13	ν_{turb}	turbulent kinematic viscosity (m ² /sec)
14	ν_{molec}	molecular kinematic viscosity (m ² /sec)
15	ρ	density (kg/m ³)
16	τ_{ij}	components of stress tensor (Pa)
17		
18		

1 **Table 1.** A summary of experimental conditions tested, and corresponding amounts of
 2 VHP decomposition in GS duct for each condition. VHP and flow rates are reported as
 3 weighted averages calculated with Eq. 1 (\pm standard deviation) from three experiments
 4 performed on different days; temperatures are simple averages between first and last
 5 absorption cells. Per cent VHP decomposition values were computed from mass balance
 6 calculations as described in text.

Experimental conditions						VHP decomp ^e
VHP, first abs cell ^a	VHP, last abs cell ^a	Avg. temp ^b	H ₂ O ₂ (l) sterilant	H ₂ O ₂ (l) vap rate ^c	flow rate	
(mg/L)	(mg/L)	(°C)	(%w/w)	(g/min)	(acmh) ^d	(mass%)
<i>Experiments at different initial concentrations (corresponds to data in Fig. 2a)</i>						
0.36 ± 0.01	0.02±0.002	29.9 ± 0.8	14	1.0	19.6 ± 0.2	95.2
0.58 ± 0.01	0.06±0.004	29.8 ± 0.8	14	1.5	20.7 ± 0.2	90.1
1.12 ± 0.03	0.20±0.01	30.2 ± 0.7	35	1.2	19.7 ± 0.2	84.2
<i>Experiments at different flow rates (corresponds to data in Fig. 3a)</i>						
0.53 ± 0.01	0.15±0.01	31.1 ± 1.1	35	1.2	46.6 ± 0.3	71.3
0.52 ± 0.01	0.23±0.01	29.7 ± 0.2	35	2.1	77.9 ± 0.3	60.2
<i>Experiments at different temperatures (corresponds to data in Fig. 4a)</i>						
1.11 ± 0.01	0.50±0.01	21.8 ± 0.6	35	1.1	19.4 ± 0.2	58.4
1.16 ± 0.16	0.02±0.003	37.8 ± 0.4	35	1.4	19.9 ± 0.2	98.6

7 ^a absorption cell

8 ^b average temperature between first and last absorption cells

9 ^c vaporization rate of H₂O₂ (l) sterilant

10 ^d actual cubic meter per hour

11 ^e VHP decomposition in GS duct

12

13

1 **Table 2.** Values of K_1 and K_2 (Eq. 7), and surface area normalized decomposition rates
2 (K_A) of VHP in GS duct, as a function of temperature tested.

3

Avg. Temp (°C)	K_1 (mg/L/sec)	K_2 (mg/L)	K_A (nmol/min/cm²)*
21.8	4.0	1.9	40
30.2	9.0	1.3	97
37.8	16	0.8	167

*nanomoles VHP/min/cm² of GS duct

4

5

6

7

1 **Literature Cited**

- 2 (1) Sharp, R. J. and Roberts, A. G. Anthrax: the challenges for decontamination. *J.*
3 *Chem. Technol. Biot.* **2006**, 81, 1612-1625.
4
- 5 (2) UCLA. Website for the Department of Epidemiology, School of Public Health,
6 University of California at Los Angeles.
7 <http://www.ph.ucla.edu/epi/bioter/bioterrorism.html>. Accessed February, 2007.
8
- 9 (3) Weis, C. P., Intrepido, A. J., Miller, A. K., Cowin, P. G., Durno, M. A., Gebhardt,
10 J. S., Bull, R. Secondary aerosolization of viable *Bacillus anthracis* spores in a
11 contaminated US Senate Office. *JAMA*, **2002**, 288(22), 2853-2858.
12
- 13 (4) Sippola, M. R. and Nazaroff, W. W. Modeling particle loss in ventilation ducts.
14 *Atmos. Environ.* **2003**, 37, 5597-5609.
15
- 16 (5) Sippola, M. R., and Nazaroff, W. W. Experiments measuring particle deposition
17 from fully developed turbulent flow in ventilation ducts. *Aerosol Sci. Tech.*
18 **2004**, 38, 914-925.
19
- 20 (6) Krauter, P., Biermann, A., and Larsen, L. D. Transport efficiency and deposition
21 velocity of fluidized spores in ventilation ducts. *Aerobiologia*. **2005**, 21, 155-
22 172.
23

- 1 (7) Sippola, M. R. and Nazaroff, W. W. Particle deposition in ventilation ducts:
2 connectors, bends, and developing turbulent flow. *Aersol Sci. Tech.* **2005**, 39,
3 139-150.
4
- 5 (8) Cummings, A. L., Childers, R. W., and Mielnik, T. J. *Flow- through vapor*
6 *phase sterilization system.* 1990, US Patent no. 4,909,999.
7
- 8 (9) Jahnke, M. and Lauth, G. Biodecontamination of a large volume filling room with
9 hydrogen peroxide. *Pharm. Eng.* **1997**, Jul-Aug, 96-108.
10
- 11 (10) Krause, J., McDonnell, G., and Riedesel, H. Biodecontamination of animal
12 rooms and heat sensitive equipment with vaporized hydrogen peroxide. *Contemp.*
13 *Top. Lab. Anim. Sci.* **2001**, 40(6), 18-21.
14
- 15 (11) Wagner, G. W., Sorrick, D. C., Procell, L. R., Brickhouse, M. D., McVey, I. F.,
16 and Schwartz, L. I. Decontamination of VX, GD, and HD on a surface using
17 modified vaporized hydrogen peroxide. *Langmuir*, **2007**, 23(3), 1178-1186.
18
- 19 (12) Edwards, S. J., Geist, S. G., and Steen, P. A. *Multiple flashpoint vaporization*
20 *system.* 2000, US Patent No. 6,077,480.
21
- 22 (13) Brickhouse, M. D., Turetsky, A., and McVey, I. F. *Decontamination of CBW*
23 *agents by mVHP: Demonstration of the CBW decontamination of a building*

1 *using mVHP*. Edgewood Chemical Biological Center technical report ECBC-TR-
2 470S, 2005.

3

4 (14) Adams, D., Brown, G. P., Fritz, C., and Todd, T. T. Calibration of a near-
5 infrared (NIR) H₂O₂ vapor monitor. *Pharm. Engin.* **1998**,18(4), 66-85.

6

7 (15) Bevington, P. R. and Robinson, D. K. *Data reduction and error analysis for the*
8 *physical sciences*, 2nd ed. New York: McGraw-Hill, 1992, p. 59.

9

10 (16) Rickloff, J. R. and Orelski, P. A. Resistance of various microorganisms to
11 vaporized hydrogen peroxide in a prototype tabletop sterilizer. In *Proceedings of*
12 *the 89th Annual Meeting of the American Society of Microbiology*. American
13 Society for Microbiology: Washington, D. C. 1989; pp. 15-21.

14

15 (17) Klapes, N. A. and Vesley, D. Vapor-phase hydrogen peroxide as a surface
16 decontaminant and sterilant. *Appl. Environ. Microb.* **1990**, 56(2), 503-506.

17

18 (18) Kokubo, M., Inoue, T., and Akers, J. Resistance of common environmental
19 spores of the genus *Bacillus* to vapor hydrogen peroxide. *PDA J. Pharm. Sci.*
20 *Tech.* **1998**, 52(5), 228-231.

21

- 1 (19) Johnston, M. D., Lawson, S., and Otter, J. A. Evaluation of hydrogen peroxide
2 vapour as a method for the decontamination of surfaces contaminated with
3 *Clostridium botulinum* spores. *J. Microbiol. Meth.* **2005**, 60(3), 403-411.
4
- 5 (20) Rogers, J. V., Sabourin, C. L. K., Choi, Y. W., Richter, W. R., Rudnicki, D. C.,
6 Riggs, K. B., Taylor, M. L., and Chang, J. Decontamination assessment of
7 *Bacillus anthracis*, *Bacillus subtilis*, and *Geobacillus stearothermophilus* spores
8 on indoor surfaces using a hydrogen peroxide gas generator. *J. Appl. Microbiol.*
9 **2005**, 99, 739-748.
10
- 11 (21) Asproulis, P. N. *High resolution numerical predictions of hypersonic flows on*
12 *unstructured meshes*. Ph.D Dissertation, Imperial College, Dept. of Aeronautics,
13 London, England, 1994.
14
- 15 (22) Patankar, S. V. *Numerical heat Transfer and Fluid Flow*. Hemisphere:
16 Washington D.C. 1980.
17
- 18 (23) Naphon, P. and Wongwises, S. A review of flow and heat transfer characteristics
19 in curved tubes. *Renew. Sust. Energ. Rev.* **2006**, 10(5), 463-490.
20
- 21 (24) Block, S. S. *Disinfection, sterilization, and preservation*, 4th ed. Lea and Febiger:
22 Philadelphia, 1991, p. 74, p. 80.
23

- 1 (25) Satterfield, C. N., and Stein, T. W. Homogeneous decomposition of hydrogen
2 peroxide vapor. *J. Phys. Chem. (US)*. **1957**, 61(5), 537-540.
- 3
- 4 (26) Hart, A. B. and Ross, R. A. Catalytic decomposition of hydrogen peroxide
5 vapour by equimolar mixed oxides. *Nature* **1962**, 193(4821), 1175-1177.
- 6
- 7 (27) Hart, A. B., McFadyen, J., and Ross, R. A. Solid-oxide-catalyzed decomposition
8 of hydrogen peroxide vapour. *T. Faraday Soc.* **1963**, 59(486), 1458-1469.
- 9
- 10 (28) Satterfield, C. N., and Stein, T. W. Decomposition of hydrogen peroxide vapor
11 on relatively inert surfaces. *Ind. Eng. Chem.* **1957**, 49(7), 1173-1180.
- 12
- 13 (29) Han, Y., Applegate, B., Linton, R. H., and Nelson, P. E. Decontamination of
14 *Bacillus thuringiensis* spores on selected surfaces by chlorine dioxide gas. *J.*
15 *Environ. Health.* **2003**, 66(4), 16-20.
- 16
- 17 (30) Morrison, G. C. and Nazaroff, W. W. The rate of ozone uptake on carpets:
18 experimental studies. *Environ. Sci. Technol.* **2000**, 34(23), 4963-4968.
- 19
- 20 (31) Swartling, P. and Lindgren, B. The sterilizing effect against *Bacillus subtilis*
21 spores of hydrogen peroxide at different temperatures and concentrations. *J.*
22 *Dairy Res.* **1968**, 35, 423-428.
- 23

- 1 (32) Toledo, R. T., Escher, F. E., and Ayres, J. C. Sporicidal properties of hydrogen
2 peroxide against food spoilage organisms. *Appl. Microbiol.* **1973**, 26(4), 592-
3 597.
- 4
- 5 (33) Berger, S. A. *Flow and heat transfer in curved pipes and tubes*. AIAA 91-0030,
6 1991, pp. 1-19.
- 7
- 8 (34) USEPA. *Compilation of available data on building decontamination alternatives*.
9 Report no. EPA/600/R-05/036, 2005, p. 124.
- 10
- 11 (35) STE. *VHP fumigation of GSA Building 410*. Strategic Technology Enterprises
12 Inc. final report. 2003. Provided by Iain F. McVey as a personal communication.
- 13
- 14 (36) Gordon, G., and Rosenblatt, A. A. Chlorine dioxide: the current state of the art.
15 *Ozone Sci. Eng.* **2005**, 27(3), 203-207.
- 16

1 **Figure Captions**

2

3 **Figure 1.** Schematic of experimental apparatus. Round GS and PVC-lined ducts were
4 constructed and tested separately, but had essentially the same configuration shown here.
5 Dimension shown indicates overall size of apparatus. Locations of near-infrared
6 absorption cells for VHP measurement (inset) were approximately 1 m, 4 m, 8 m, 13 m,
7 20 m, and 27 m from the inlet.

8

9 **Figure 2.** Effect of initial concentration on VHP profiles in GS (*a*) and PVC-lined steel
10 (*b*) ducts, respectively, and CFD predictions of VHP concentrations in GS duct (dotted
11 lines in (*a*)). Nominal conditions were ~21 acmh and ~30°C; see Table 1 for exact
12 values. Each symbol is a weighted average (calculated via Eq. 1) of VHP concentrations
13 from a given absorption cell (\pm standard deviation as error bars) for triplicate experiments
14 performed on separate days. Data from the PVC-lined duct were not modeled with CFD
15 and are connected with solid lines (*b*).

16

17 **Figure 3.** Effect of flow rate on VHP profiles in GS and PVC-lined steel (inset) ducts,
18 and CFD predictions of VHP concentrations in GS duct (dotted lines). Nominal
19 conditions were ~30°C and ~0.55 mg/L at the first absorption cell; see Table 1 for exact
20 values. Data at 21 acmh (\square) are reproduced from Fig. 2a for ease of comparison. See
21 caption of Figure 2 for additional remarks.

22

1 **Figure 4.** Effect of temperature on VHP profiles in GS and PVC-lined steel (inset) ducts,
2 and CFD predictions of VHP concentrations in GS duct (dotted lines). Nominal
3 conditions were ~21 acmh and ~1.1 mg/L at the first absorption cell; see Table 1 for
4 exact values. Data at 30°C (O) are reproduced from Fig. 2a for ease of comparison. See
5 caption of Figure 2 for additional remarks.

6

7 **Figure 5.** The effect of bends on VHP concentration. Panel (a) shows the VHP
8 concentration profile estimated by CFD at 0.6 m before (solid line) and 0.3 m after
9 (dotted line) the first bend in the duct. The abscissa in (a) is the axial distance across the
10 duct. Panel (b) shows the overall effect of bends, comparing a CFD simulation of the
11 actual GS duct tested (dotted line; reproduced from Fig. 2a) with a simulation of a
12 straight duct with no bends (solid line) of the same total length.

13

14 **Figure 6.** Comparison between CFD-predicted bulk and surface concentrations in the GS
15 duct. The surface concentration (solid line) is for an arbitrary line run along the length of
16 the duct; the bulk concentration (dotted line) is reproduced from Fig. 2a. The oscillations
17 in surface concentrations (solid line) are due to locally lower VHP concentrations
18 experienced on the inner edge of some bends, and locally higher concentrations on the
19 outer edge of other bends.

20

21 **Figure 7.** Kill of *G. stearothermophilus* BIs placed in the immediate vicinity of the first
22 (a) and fifth (b) absorption cells in the GS duct, at nominal conditions of ~ 30°C and ~ 20
23 acmh flow rate. Results are expressed at the per cent of BIs that were positive for growth

1 at the corresponding $C \cdot t$ value. Symbols are averages (\pm standard deviation as error bars)
2 from triplicate experiments in which 10 BIs were used per experiment. Surface VHP
3 concentrations given in each panel were obtained from CFD.

4

5 **Figure 8.** Estimated fractional decontamination of the GS duct, for the highest flow rate
6 (*curve a*) and highest initial VHP concentration (*curve b*) tested. Decontamination was
7 estimated as the fraction of the duct's surface that exceeded a $C \cdot t$ value of 100 mg/L \cdot min
8 for a given exposure time step.

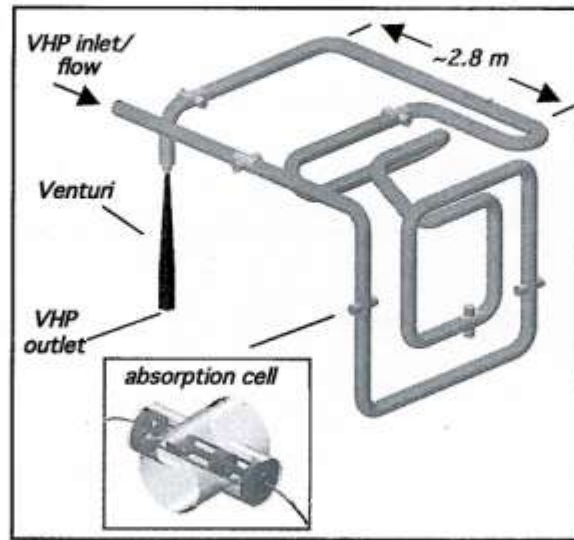


Figure 1. Schematic of experimental apparatus. Round GS and PVC-lined ducts were constructed and tested separately, but had essentially the same configuration shown here. Dimension shown indicates overall size of apparatus. Locations of near-infrared absorption cells for VHP measurement (inset) were approximately 1 m, 4 m, 8 m, 13 m, 20 m, and 27 m from the inlet.

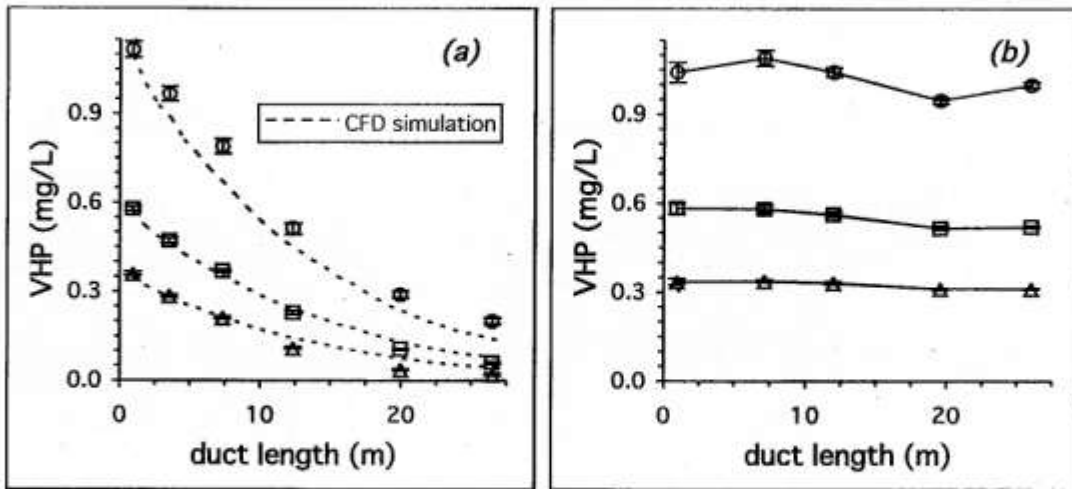


Figure 2. Effect of initial concentration on VHP profiles in GS (a) and PVC-lined steel (b) ducts, respectively, and CFD predictions of VHP concentrations in GS duct (dotted lines in (a)). Nominal conditions were ~ 21 acmh and $\sim 30^\circ\text{C}$; see Table 1 for exact values. Each symbol is a weighted average (calculated via Eq. 1) of VHP concentrations from a given absorption cell (\pm standard deviation as error bars) for triplicate experiments performed on separate days. Data from the PVC-lined duct were not modeled with CFD and are connected with solid lines (b).

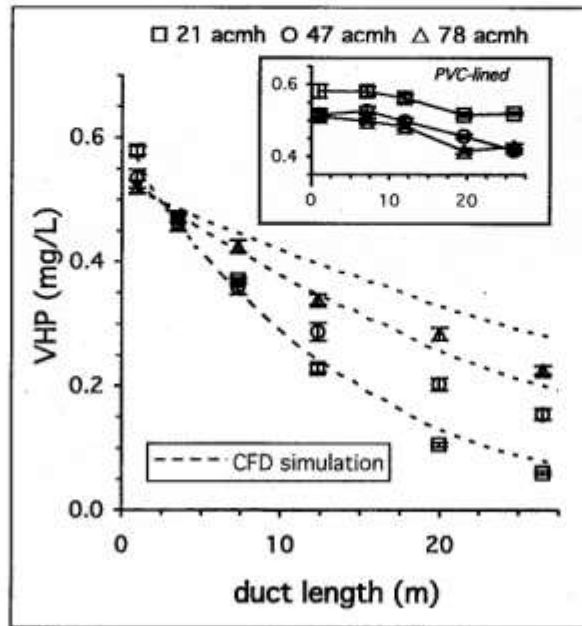


Figure 3. Effect of flow rate on VHP profiles in GS and PVC-lined steel (inset) ducts, and CFD predictions of VHP concentrations in GS duct (dotted lines).

Nominal conditions were $\sim 30^{\circ}\text{C}$ and ~ 0.55 mg/L at the first absorption cell; see Table 1 for exact values. Data at 21 acmh (\square) are reproduced from Fig. 2a for ease of comparison. See caption of Figure 2 for additional remarks.

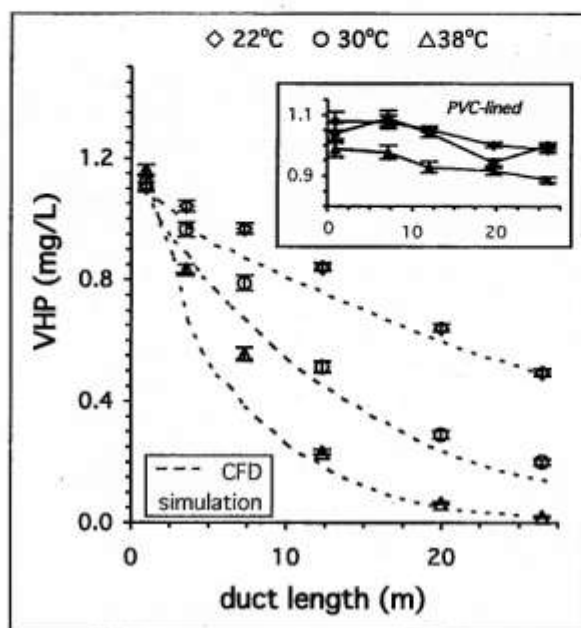


Figure 4. Effect of temperature on VHP profiles in GS and PVC-lined steel (inset) ducts, and CFD predictions of VHP concentrations in GS duct (dotted lines). Nominal conditions were ~ 21 acmh and ~ 1.1 mg/L at the first absorption cell; see Table 1 for exact values. Data at 30°C (O) are reproduced from Fig. 2a for ease of comparison. See caption of Figure 2 for additional remarks.

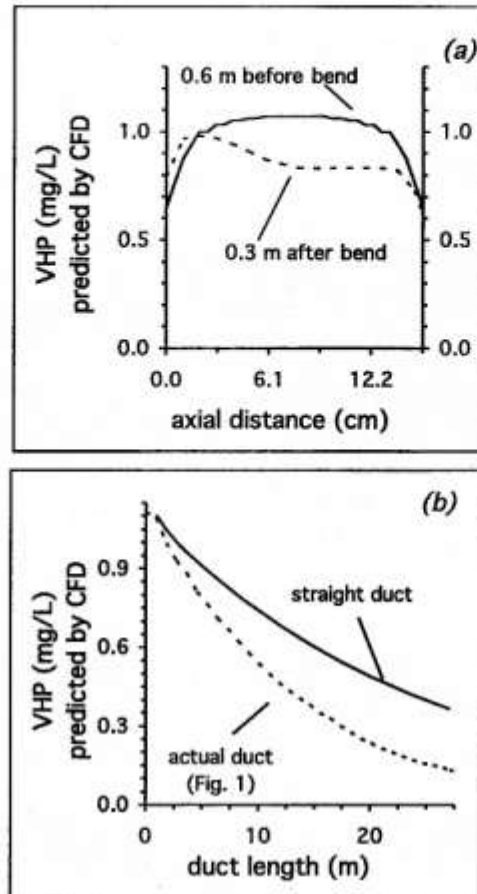


Figure 5. The effect of bends on VHP concentration. Panel (a) shows the VHP concentration profile estimated by CFD at 0.6 m before (solid line) and 0.3 m after (dotted line) the first bend in the duct. The abscissa in (a) is the axial distance across the duct. Panel (b) shows the overall effect of bends, comparing a CFD simulation of the actual GS duct tested (dotted line; reproduced from Fig. 2a) with a simulation of a straight duct with no bends (solid line) of the same total length.

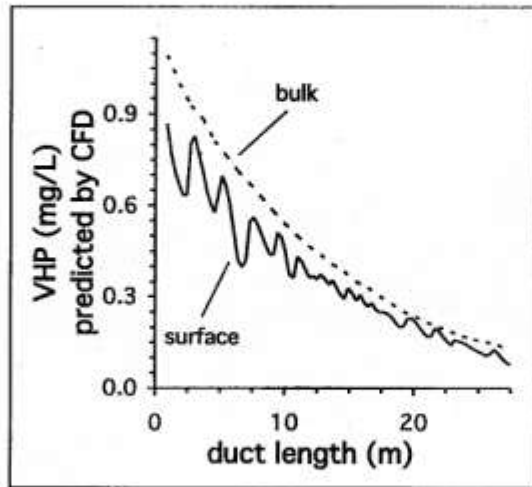


Figure 6. Comparison between CFD-predicted bulk and surface concentrations in the GS duct. The surface concentration (solid line) is for an arbitrary line run along the length of the duct; the bulk concentration (dotted line) is reproduced from Fig. 2a. The oscillations in surface concentrations (solid line) are due to locally lower VHP concentrations experienced on the inner edge of some bends, and locally higher concentrations on the outer edge of other bends.

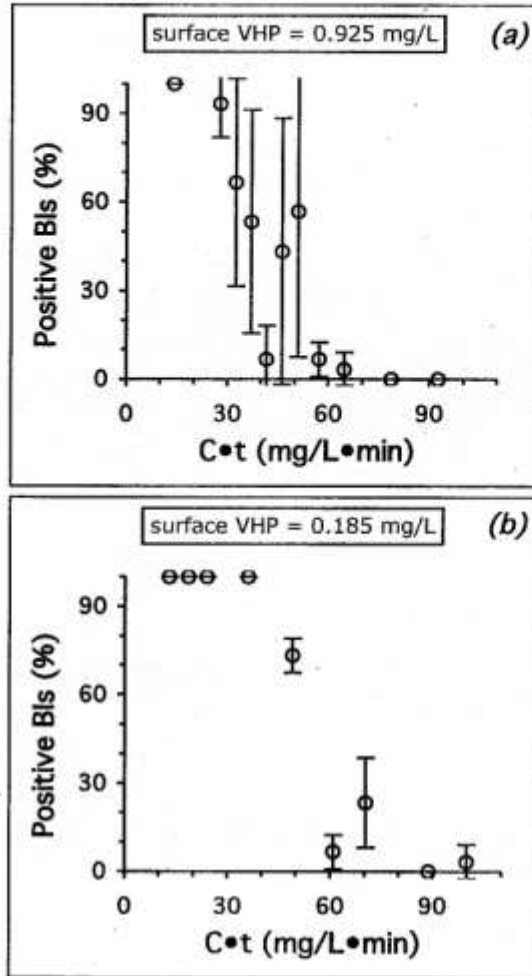


Figure 7. Kill of *G. stearotherophilus* BIs placed in the immediate vicinity of the first (a) and fifth (b) absorption cells in the GS duct, at nominal conditions of $\sim 30^{\circ}\text{C}$ and ~ 20 acmh flow rate. Results are expressed at the per cent of BIs that were positive for growth at the corresponding C•t value. Symbols are averages (\pm standard deviation as error bars) from triplicate experiments in which 10 BIs were used per experiment. Surface VHP concentrations given in each panel were obtained from CFD.

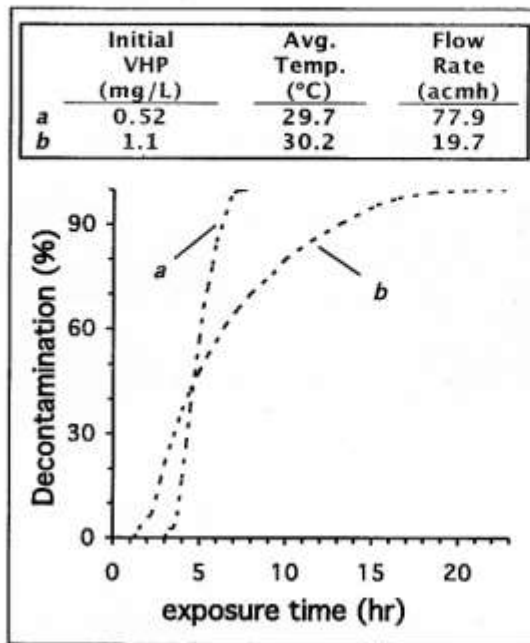


Figure 8. Estimated fractional decontamination of the GS duct, for the highest flow rate (*curve a*) and highest initial VHP concentration (*curve b*) tested. Decontamination was estimated as the fraction of the duct's surface that exceeded a $C \cdot t$ value of 100 mg/L•min for a given exposure time step.

SUPPORTING INFORMATION FOR:

**MINIMIZING DECOMPOSITION OF VAPORIZED HYDROGEN PEROXIDE
IN CLEAN GALVANIZED STEEL DUCTING:
IMPLICATIONS FOR BIOLOGICAL DECONTAMINATION**

MATTHEW F. VERCE,^{*†§} BUVANESWARI JAYARAMAN,[‡] TIMOTHY D.
FORD,^{†§} SCOTT E. FISHER,^{†§} ASHOK J. GADGIL,[‡] AND TINA M. CARLSEN[#]
Environmental Restoration Division, National Security Engineering Division, and
Biosciences and Biotechnology Division, Lawrence Livermore National Laboratory,
Livermore CA 94551 and Environmental Energy Technologies Division, Lawrence
Berkeley National Laboratory, Berkeley, CA 94720

* Corresponding author. Mailing address: L-530, Lawrence Livermore National
Laboratory, Livermore CA 94551. Phone: (925) 423 – 2129. Fax: (925) 424 – 3155.
Email: vercel@llnl.gov

† Environmental Restoration Division, Lawrence Livermore

‡ Environmental Energy Technologies Division, Lawrence Berkeley

§ National Security Engineering Division, Lawrence Livermore

Biosciences and Biotechnology Division, Lawrence Berkeley

CONTENTS

Additional details on the experimental apparatus.

Additional details of CFD modeling.

Additional details on the effect of bends on decomposition.

Additional details on the experimental apparatus. Decontamination experiments were conducted in two adjacent rooms of a retrofitted construction trailer, housing a model duct run and required instrumentation, respectively. VHP produced by a STERIS VHP 1000[®] generator (residing in the adjacent room) was passed through a ~15 m coil of 2 in (5.1 cm) braided Tygon[®] tubing, to cool the vapor to experimental temperature prior to introducing it into the duct. VHP concentrations were measured in real time at six locations along the duct (Fig. 1) with a Guided Wave Model 412 Process Analyzer, which measures VHP and water vapor concentrations by near-infrared spectroscopy (Adams et al., 1998). Absorption cells (25 cm path length) were placed normally to the duct's axis (inset, Fig. 1), and transmitted absorbance spectra via 10 m fiber optic cables to the analyzer in the adjacent room for measurement. Temperature at each absorption cell was measured by a thermistor (Omega, model THX400AP) protruding into the duct. A flow straighter constructed of ~470 beverage straws was inserted into the ductwork ~1 m upstream of the first absorption cell, to impart a laminar velocity profile on the flow at the start of the duct. Flow rates were measured by two,

separate “machined convergent” type venturis manufactured to the standard ASME MFC-3M-1989 (ASME, 1989), having beta values of 0.3030 (for majority of experiments performed at ~21 actual cubic meter per hour (1 acmh \approx 12 actual cubic feet per minute) or 0.6282 (for higher flow rates), and estimated discharge coefficients greater than 0.95 (ASME, 1937). Pressure differences from the venturis were measured by a differential pressure transmitter (Dwyer, model 607-0). VHP data were recorded by proprietary software provided with the near-infrared instrument, and all temperature and flow data were recorded in real time by a computer data acquisition program written in LabVIEW 6.0.1.

For the majority of experiments run at a nominal flow rate of ~21 acmh, the VHP 1000[®] generator was used as the source of flow, by connecting it in a closed loop with the duct. The VHP 1000[®]'s internal catalytic converter removed remaining VHP in the return stream before infusing it with freshly vaporized sterilant, providing a constant mass loading of VHP into the duct. Higher flow rates were tested separately in a “one pass” experiment, in which conditioned outside air was pulled through the duct with a dust collector (Dayton model 6H004A) attached to its outlet, and then exhausted outside after passing through a fluidized bed of palladium beads. For these experiments, the generator injected VHP into the beginning of the duct, and was provided a separate source of return air.

Additional details of CFD modeling. CFD simulation of the loss of VHP within the GS duct was performed using the commercial software STAR-CD (Adapco, 2004) using the second-order Monotone Advection Reconstruction Scheme (Asproulis, 1994) and the SIMPLE algorithm (Patankar, 1980). A computational grid consisting of 817,000

cells was constructed for the duct configuration shown in Fig. 1. Local mesh refinement was carried out close to the walls, resulting in a maximum non-dimensional normal distance (y^+) from the wall of 0.6. The finite volume formulation of the Reynolds Averaged Navier Stokes equations were solved to predict the steady-state airflow field in the duct

$$\frac{\partial U_j}{\partial x_j} = 0 \quad (S1)$$

$$U_j \frac{\partial U_i}{\partial x_j} = -\frac{1}{\rho} \frac{\partial p}{\partial x_i} + \frac{\partial}{\partial x_j} \left(\nu_{total} \frac{\partial U_i}{\partial x_j} \right) + \frac{\partial \tau_{ij}}{\partial x_j} \quad (S2)$$

Turbulence was included via stress tensor elements τ_{ij} , determined by integrating the low-Reynolds-number turbulence model

$$U_j \frac{\partial k}{\partial x_j} = \frac{\partial}{\partial x_j} \left(\nu_{total} \frac{\partial k}{\partial x_j} \right) + \nu_{turb} P - \epsilon \quad (S3)$$

$$U_j \frac{\partial \epsilon}{\partial x_j} = \frac{\partial}{\partial x_j} \left(\nu_{molec} + \frac{\nu_{turb}}{1.22} \frac{\partial \epsilon}{\partial x_j} \right) + \frac{\epsilon}{k} 1.44 \nu_{turb} (P + P') - 1.92 \left(1 - 0.3e^{-R_i^2} \right) \frac{\epsilon^2}{k} \quad (S4)$$

all the way to the wall of the duct, as opposed to assuming a wall function. The stress tensor τ_{ij} (Eq. S2) is given by:

$$\tau_{ij} = \nu_{total} \left(\frac{\partial U_i}{\partial x_j} + \frac{\partial U_j}{\partial x_i} \right) - \overline{\rho U_i U_j} \quad (S5)$$

ν_{total} is the total kinematic viscosity given by:

$$\nu_{total} = \nu_{turb} + \nu_{molec} \quad (S6)$$

ν_{turb} (Eqs. S3-S4) is the turbulent viscosity and is calculated using the expression

$$\nu_{turb} = f_{\mu} \frac{0.09\rho k^2}{\varepsilon} \quad (S7)$$

$$\text{where } f_{\mu} = \left(1 - e^{-0.0198 Re_y}\right) \left(1 + \frac{5.29}{Re_y}\right) \text{ and } Re_y = y\sqrt{k}/\nu \quad (S8); (S9)$$

where y is the normal distance to the wall. R_t (Eq. S4) is the turbulent Reynolds number given by

$$R_t = k^2/\nu\varepsilon \quad (S10)$$

P (Eqs. S3-S4) is the production of k by mean velocity gradients given by

$$P = \left(\frac{\partial U_i}{\partial x_j} + \frac{\partial U_j}{\partial x_i}\right) \frac{\partial U_i}{\partial x_j} \quad (S11)$$

and P' (Eq. S4), which ensures that the correct level of near-wall turbulence energy dissipation is returned, is given by

$$P' = 1.33 \left(1 - 0.3e^{-R_t^2}\right) \left(P + 2 \frac{\mu_{molec}}{\mu_{turb}} \frac{k}{y^2}\right) e^{-0.00375 Re_y^2} \quad (S12)$$

Lastly, the VHP concentrations were predicted for a given airflow field by solving the transport equation

$$U_j \frac{\partial C}{\partial x_j} + \frac{\partial}{\partial x_j} \left(CV_{m,j} + \overline{u'_j C'}\right) = S \quad (S13)$$

where S is the sink term due to VHP decomposition, which was set equal to

$$S = -\frac{K_1 C}{K_2 + C} \quad (\text{S14})$$

in the first layer of cells adjacent to the wall, and zero everywhere else. The mixed order form of Eq. S14 was suggested by data collected at different initial VHP concentrations (see Results section of manuscript), which indicated a uniform loss rate at the highest concentrations tested, and a first order loss at lower concentrations. Several simulations of each VHP data set were performed, until one set of values for K_1 and K_2 was obtained that resulted in an acceptable root mean square error. All terms in the above equations are summarized below.

Calculations were performed on a dual AMD Athlon 2200+ Linux cluster using 4 dual processor nodes. The airflow field (Eqs. S1-S4) and transport (Eqs. S13-14) equations were considered converged when their normalized residuals fell below 1E-4 and 1E-10, respectively, which required between 12-42 hours and 2-3 hours of CPU time, respectively. A comparison of predicted velocity profiles as the airflow transitioned from the inlet plane (laminar plug flow) into a fully developed turbulent pipe flow provided verification that the airflow was being modeled as expected (data not shown).

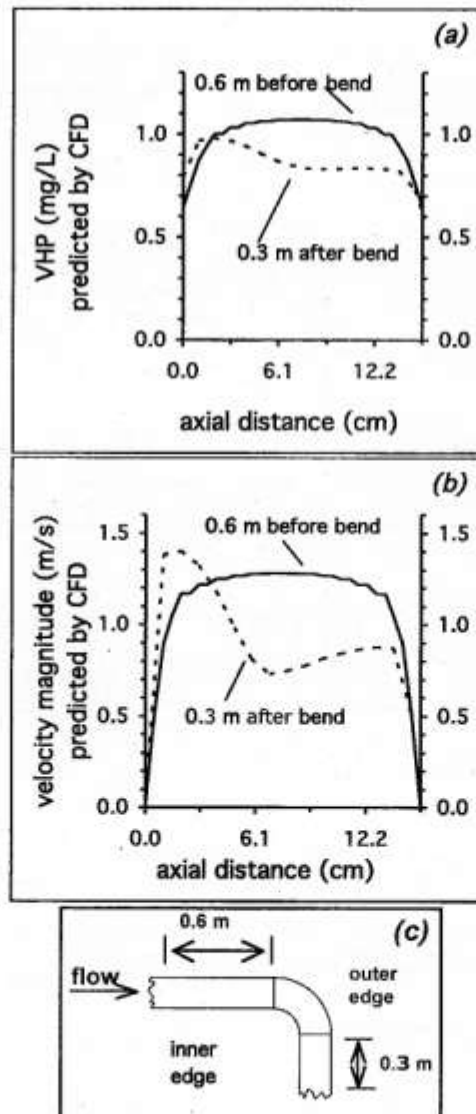
Terms used in these equations are defined below:

C concentration of VHP (mg/L)

\bar{C}_i steady state average VHP concentration from a given experiment

C'	fluctuating components of concentration
k	turbulent kinetic energy (m^2/sec^2)
P	production of turbulent kinetic energy k , by mean velocity gradients
P'	near-wall turbulence energy dissipation
p	pressure (Pa)
R_t	turbulent Reynolds number
s_i	standard deviation of VHP concentration from a given experiment
t	time (sec)
u'_i	fluctuating velocity component (m/sec)
U_i	mean velocity component (m/sec)
$V_{m,j}$	diffusion velocity component (m/sec)
x_i	Cartesian coordinate ($i=1, 2, 3$) (m)
y^*	non-dimensional normal distance from the wall
ε	turbulent dissipation rate (m^2/sec^3)
ν_{total}	total kinematic viscosity (m^2/sec)
ν_{turb}	turbulent kinematic viscosity (m^2/sec)
ν_{molec}	molecular kinematic viscosity (m^2/sec)
ρ	density (kg/m^3)
τ_{ij}	components of stress tensor (Pa)

Additional details on the effect of bends on decomposition. The following figure is an enhanced version of Fig. 5 in the published manuscript, which shows additional data on the velocity profile before and after the first bend, and a schematic defining where the “entering” and “exiting” profiles were taken. Panel (a) shows the VHP concentration profile estimated by CFD at 0.6 m before (solid line) and 0.3 m after (dotted line) the first bend in the duct. Panel (b) shows the CFD estimated velocity magnitude profile at the same locations. The abscissa of (a) and (b) is the axial distance across the duct, with the outer edge of the duct at 0 cm, and the inner edge at 15.24 cm (6 in), as indicated in schematic (c).



Literature Cited

Adams, D., Brown, G. P., Fritz, C., and T. T. Todd. 1998. Calibration of a near- infrared (NIR) H₂O₂ vapor monitor. *Pharm. Engin.* 18(4): 66-85.

Adapco. 2004. Star-CD Version 3.2 Methodology. (Adapco, Inc).

Asproulis, P. N. 1994. High resolution numerical predictions of hypersonic flows on unstructured meshes. Ph.D Dissertation, Imperial College, Dept. of Aeronautics, London, England.

ASME. 1937. Fluid meters: their theory and application, Part 1. 4th ed. (New York: The American Society of Mechanical Engineers.)

ASME. 1989. Measurement of fluid flow in pipes using orifice, nozzle, and venturi. Standard no. ASME MFC-3M—1989.

Patankar, S. V. 1980. Numerical heat Transfer and Fluid Flow. (Washington D.C: Hemisphere).